Journal of Structural Geology, Vol. 13, No. 3, pp. 281 to 297, 1991
Printed in Great Britain

0191-8141/91 $03.00+0.00

Planar dispersion of folds in ductile shear zones and kinematic interpretation of fold-hinge girdles

JONATHAN W. MIES*

Department of Geology, University of North Carolina, Chapel Hill, NC 27599-3315, U.S.A.

(*Received* 3 *July* 1989; *accepted in revised form* 25 *June* 1990)

Abstract—As indicated by theory and multiple case studies, hinge lines of minor folds in ductile shear zones are dispersed in a plane that is incompletely rotated toward mylonitic foliation. This yields a geometric relationship between the fold-hinge girdle and mylonitic foliation that can be used to determine sense of shear.

Statistical study of published data from various shear zones and of new data from the Blue Ridge thrust complex reveals a small to moderate angle between the best-fit plane to hinge lines and mean mylonitic foliation. This angle is 4–9° in eight of 12 test cases. Moderate angles, 22–34°, are associated with nappes. Kinematic analyses of 12 fold-hinge girdles indicate the sense of shear otherwise determined for host shear zones.

A theoretical model of contemporary fold rotation in simple shear closely simulates the geometric relationships described above for natural folds. Using this model, large shear strains ($\gamma \geq 10$) are implied by the 4–9° angle between the fold-hinge girdle and mylonitic foliation.

INTRODUCTION

HINGE LINES of minor folds in ductile shear zones are commonly dispersed in a plane. In spherical projection, this is evident as a *fold-hinge girdle* (e.g. Christie 1963, Carreras *et al.* 1977, Williams 1978, Evan & White 1984, Faure 1985, Boyle 1987). Girdle-distributed folds include a variety of geometries and styles illustrated by Lindström (1961, Fig. 1). Bryant & Reed (1969) attributed similar relationships to tightening and passive rotation of open folds, formed early during thrusting, toward the transport direction. Many subsequent studies have analyzed fold rotation during irrotational strain (Borradaile 1972, Sanderson 1973, Ramsay 1979), simple shear (Escher & Watterson 1974, Carreras *et al.* 1977, Williams 1978), and the general case of combined irrotational strain and simple shear (Ramberg & Ghosh 1977).

Various aspects of the fold-hinge girdle were explored by Hansen (1971, p. 33), who recognized what he termed the *separation angle*—the angular gap in the girdle between folds of opposing vergence (i.e. 'S' and 'Z' asymmetries). Rotation and geometric modification of folds in shear zones have been described in the literature (e.g. Carreras *et al.* 1977, Fossen & Rykkelid 1990) and have been used for shear strain analysis (Bak *et al.* 1975, Grocott & Watterson 1980). However, other than in cases in which the fold-hinge girdle and mylonitic foliation were considered coplanar (e.g. Williams 1978, Michard *et al.* 1984, Vauchez *et al.* 1987), none of the previous work has specifically addressed the geometric relationship between these planes. This relationship is the focus of the present paper and it is used herein for sense-of-shear determination. The method and examples of its application are presented. A theoretical model for passive rotation of contemporary folds due to simple shear is used to simulate the development of natural fold-hinge girdles and to predict the geometric relationship observed between the best-fit plane to hinge lines and mean mylonitic foliation. The model is tested against published data and new data from the Blue Ridge thrust complex of the southern Appalachians.

In the following section, observations from the Blue Ridge thrust complex are described only as far as they pertain to the kinematic model for fold-hinge girdles. The regional significance of present interpretations is not presented.

FOLDS FROM THE BASEMENT–ASHE BOUNDARY ZONE, BLUE RIDGE THRUST COMPLEX, SOUTHERN APPALACHIANS

General geology of the Blue Ridge thrust complex

The Blue Ridge belt is part of the southern Appalachian orogen (Fig. 1). Seismic data suggest that a décollement places allochthonous Precambrian crystalline rocks of the Blue Ridge and the physiographic Piedmont over Paleozoic rocks that crop out to the northwest in the Valley and Ridge (Cook *et al.* 1979, Harris & Bayer 1979). This interpretation also roots the Brevard fault zone, which marks the southeast boundary of the Blue Ridge, in the décollement.

Many authors (e.g. Bryant & Reed 1970, Rankin 1970, Butler 1973) have considered the 'Blue Ridge thrust sheet' to comprise Grenville basement and upper Precambrian to early Paleozoic metasedimentary rocks that lie above the Linville Falls fault (i.e. exclusive of rocks exposed in the Grandfather Mountain and Mountain City windows). More recent research indicates that there may be fault-bounded subdivisions within the Blue Ridge thrust sheet (e.g. Rankin 1975, Hatcher 1978,

*Present address: Geological Survey of Alabama, 420 Hackberry Lane, P.O. Box O, Tuscaloosa, AL 35486-9780, U.S.A.

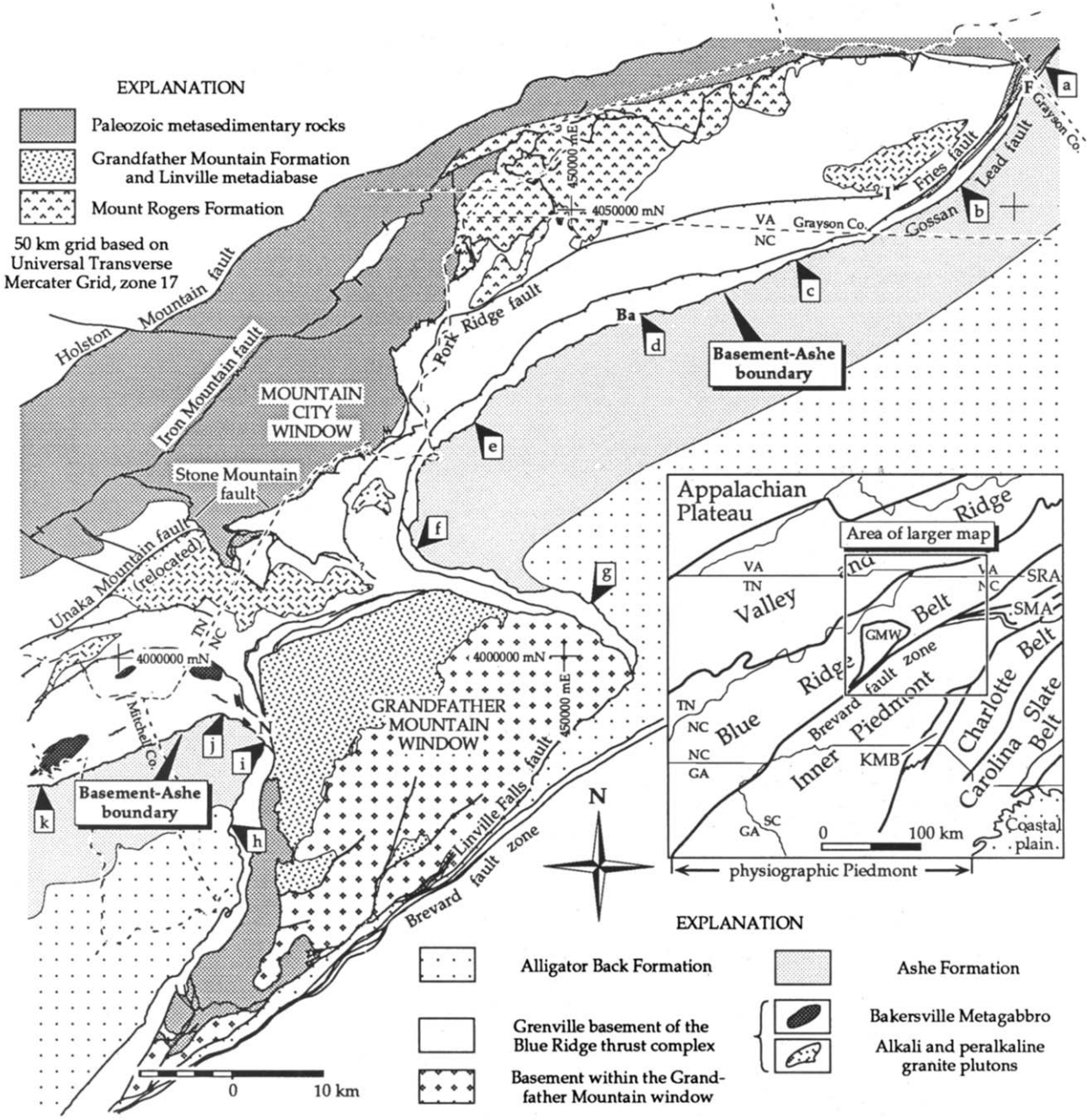

Fig. 1. Simplified geologic map of the Blue Ridge in northwestern North Carolina and adjacent states. Geology compiled with modification from the following sources: Stose & Stose (1957), King & Ferguson (1960), Bryant & Reed (1970), Rankin *et al.* (1972), Bartholomew & Lewis (1984), North Carolina Geologic Survey (state geologic map, 1985). Lower case characters (a–k, in boxes) delineate segments of the basement–Ashe boundary zone (see Fig. 2). **F** = Fries, VA; **I** = Independence, VA; **Ba** = Bina, NC; **N** = Newland, NC. Inset shows location of larger map and major geologic subdivisions of the southern Appalachians (modified after Hatcher 1978, Glover *et al.* 1983, and North Carolina Geologic Survey 1985). **GMW** = Grandfather Mountain window, **KMB** = Kings Mountain belt, **SMA** = Sauratown Mountains anticlinorium, **SRA** = Smith River allochthon.

Butler *et al.* 1987, Raymond *et al.* 1989) and inspires the designation *Blue Ridge thrust complex*. In the present report, a major thrust is recognized at the boundary between Grenville basement and the overlying Ashe Formation, a thick sequence of multiply deformed upper Precambrian(?) metasedimentary and metavolcanic rocks (Rankin 1970, Butler 1972) (Fig. 1).

Nature of the basement–Ashe boundary

The boundary between Grenville basement and the Ashe Formation has been described as a broad transitional zone (e.g. Wilcox & Poldervaart 1958, Eckelman & Kulp 1956). Bryant & Reed (1970, plate 1) mapped this zone as a unit of "mixed rocks". In the present interpretation, the mixed character of the boundary zone is ascribed to tectonic intercalation of basement and Ashe lithologies within a thrust-related ductile shear zone. Interpretation of the basement–Ashe boundary as a thrust is not new (Stose & Stose 1957, Abbott & Raymond 1984), but is controversial. The boundary has also been interpreted as a nonconformity (Rankin 1969, 1971, Rankin *et al.* 1972, 1973). Data presented here support the interpretation of Stose & Stose (1957), in which the Fries fault and the closely associated Gossan Lead fault (Fig. 1) comprise a

ductile shear zone at the basement–Ashe boundary in Grayson County, Virginia. Abbott & Raymond (1984) reviewed additional evidence for a fault, including metamorphic discontinuity, truncation of units in the Ashe and the nearly exclusive occurrence of ultramafic bodies in the Ashe (and overlying Alligator Back Formation). Mylonite at the basement–Ashe boundary in Grayson County, Virginia, was described by Stose & Stose (1957) and is described from a greater length of the boundary in the following section, as are associated mesoscopic structures.

Present study

The present structural analysis is based largely on mapping and structural data collected along 160 km of the basement–Ashe boundary from Grayson County, Virginia, to Mitchell County, North Carolina (Fig. 1). Approximately 200 oriented samples were collected during this work and have been analyzed petrographically.

A ductile shear zone as much as 1 km thick is developed primarily in the basement, immediately below the Ashe Formation. Internally, the shear zone consists of mylonite that bears all gradations of L–S shape fabric (Flinn 1965). A mineral stretching lineation in the plane of mylonitic foliation trends NW–SE and is interpreted as the transport direction. All mesoscopic structures observed are consistent with top-to-NW thrust displacement.

Structural data from the basement–Ashe boundary zone are summarized in Fig. 2. The boundary has been divided into segments of similar orientation (ab–jk, Fig. 1) to reduce complexities due to regional folds.

Rock fabric

Principal elements of rock fabric within the basement–Ashe boundary zone include gneissosity (compositional layering, S_L), schistosity (S_S), shear bands (S_B), mylonitic foliation (S_M), and stretching (mylonitic) lineation (L_M). As described below, S_M and L_M occur primarily in orthomylonite (i.e. mylonite developed from basement gneiss, and from metagranite and metagabbro that intruded the basement).

L_M is a lineation that is typically due to both flattening and elongation of mineral aggregates. This lineation lies in the plane of S_M with consistent NW–SE trend. It is most pronounced in mylonite developed from metagabbro and metagranite protoliths, in which large feldspars have been stretched and recrystallized. L-tectonite, with rod-like lineation, occurs locally and is suggestive of constrictive strain, though such a strain path is difficult to place in the context of a shear zone.

S_M is defined by spaced cleavage and compositional layering. In protomylonite and mylonite (usage of Sibson 1977), it is deflected around porphyroclasts in fluxion structure. Feldspar porphyroclasts are most common and many have tails (σ-type, Passchier & Simpson 1986) that stream in the shear direction (top-to-NW, bottom-to-SE) (Fig. 3a). In ultramylonite, S_M is spaced at mm-scale and is extremely planar, giving the weathered or broken rock a platy character. Mylonitic foliation closely parallels S_L in overlying Ashe lithologies and is observed at many localities to grade into S_L in basement gneiss (protomylonitic flaser gneiss), suggesting that these foliations are cogenetic. However, strongly discordant S_L is observed locally in the basement, where it may be related to earlier (Grenville) orogenesis (see Gulley 1985).

Mica-rich compositional layers in basement-derived mylonite commonly have an intrafolial schistosity (S_S) that is oblique to mylonitic foliation (S_M) and contains sigmoidal mica 'fish' (Lister & Snoke 1984) (Fig. 3c). A similar geometry of composite fabric occurs locally at the base of the Ashe Formation, where schistosity in mica schist is cut obliquely and is deflected by shear bands (Simpson 1986) (S_B) that are regularly spaced at cm-scale (Fig. 3d). Numerous quartz lenticles nested in schistosity are similarly sigmoidal. Surfaces of composite fabric, particularly S_B, display lineations that are approximately parallel to L_M and are perpendicular to intersections of the composite fabric. This suggests a cogenetic (or coevolutionary) relationship between S_S and S_B, and between the composite fabric ($S_S + S_B$) and L–S fabric in orthomylonite. The geometric relationships of S_S to S_B and of S_S to S_M are consistent with top-to-NW displacement (e.g. Berthé *et al.* 1979, Simpson 1986).

'Mylonitic foliation' (S_M) is distinguished from S_L by reduction of grain size, by its extreme planarity and close spacing at advanced stages of development, and most importantly by the development of stretching lineation and structures suggestive of non-coaxial deformation (i.e. composite planar fabric, asymmetric intrafolial folds, and σ-type geometry of tails on lithic clasts and porphyroclasts). However, from present observations, the genesis of S_M is uncertain; at least two possibilities must be considered. S_M may be the XY plane of finite strain associated with simple shear as in the Ramsay & Graham (1970) model, in which case L_M is the X direction. Alternatively, S_M is a shear plane foliation (cf. 'C' planes of Berthé *et al.* 1979, Lister & Snoke 1984) analogous to cards in a card deck model of simple shear (Ramsay & Huber 1983), in which case L_M is the shear direction and approximates the X direction only at high strains. It is also possible that S_M starts as the flattening plane and that layer-parallel shear along S_M initiates after sufficient rotation of the foliation toward the mechanically preferred shear plane.

Because the genesis and evolution of S_M and L_M is uncertain, the exact relationship between rock fabric and the principal strain directions is also uncertain. For purposes of structural description and kinematic analysis, S_M is assumed to contain Y and L_M is assumed to be orthogonal to Y, approximately or precisely parallel to X, such that the XZ (principal) section is perpendicular to S_M and parallel to L_M.

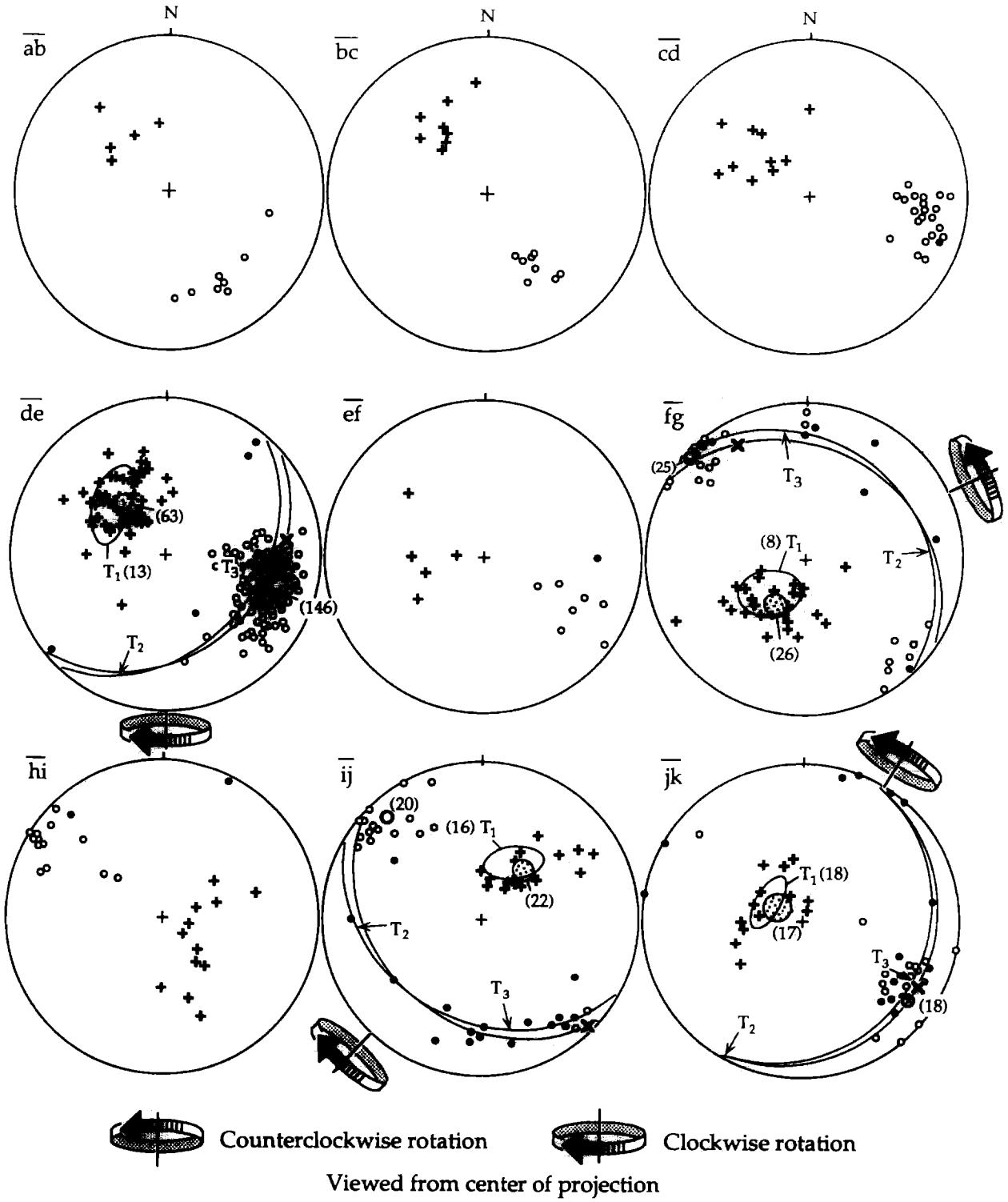

Fig. 2. Lower-hemisphere equal-area projections of structural data from segments ab–jk of the basement–Ashe boundary zone (see Fig. 1). Open circles = stretching lineations, filled circles = fold hinge lines, +s = poles to mylonitic foliation. Projections for segments de, fg, ij and jk also show mean mylonitic foliation (great circle and 95% confidence cone for pole, stippled), best-fit plane to fold hinge girdles with intermediate and maximum eigenvectors (T_2, T_3), 95% confidence cone (open) for minimum eigenvector (T_1), mean stretching lineation (bold open circle), 'calculated shear direction' (✖, see Discussion), and the interpreted sense of (incomplete) rotation of the fold-hinge girdle (see Table 1). The number of data included in each statistical parameter is shown in parentheses.

Folds

Within the basement–Ashe boundary zone, cm- to m-scale folds of S_M and S_L are common. These folds are characteristically non-parallel with relatively thick hinges and attenuated limbs, and are disharmonic to the extreme of being intrafolial. Isoclinal folds have 'S' and 'Z' asymmetries and remarkably linear hinge lines that closely parallel L_M (Fig. 4a). Relatively open folds are non-cylindrical, NW-vergent and have hinge lines that lie at a high angle to L_M (Fig. 4b). Isoclines of apparent high cylindricity may be portions of sheath folds, the axial culminations of which are not exposed (Rhodes & Gayer 1977, La Tour 1981, Evans & White 1984).

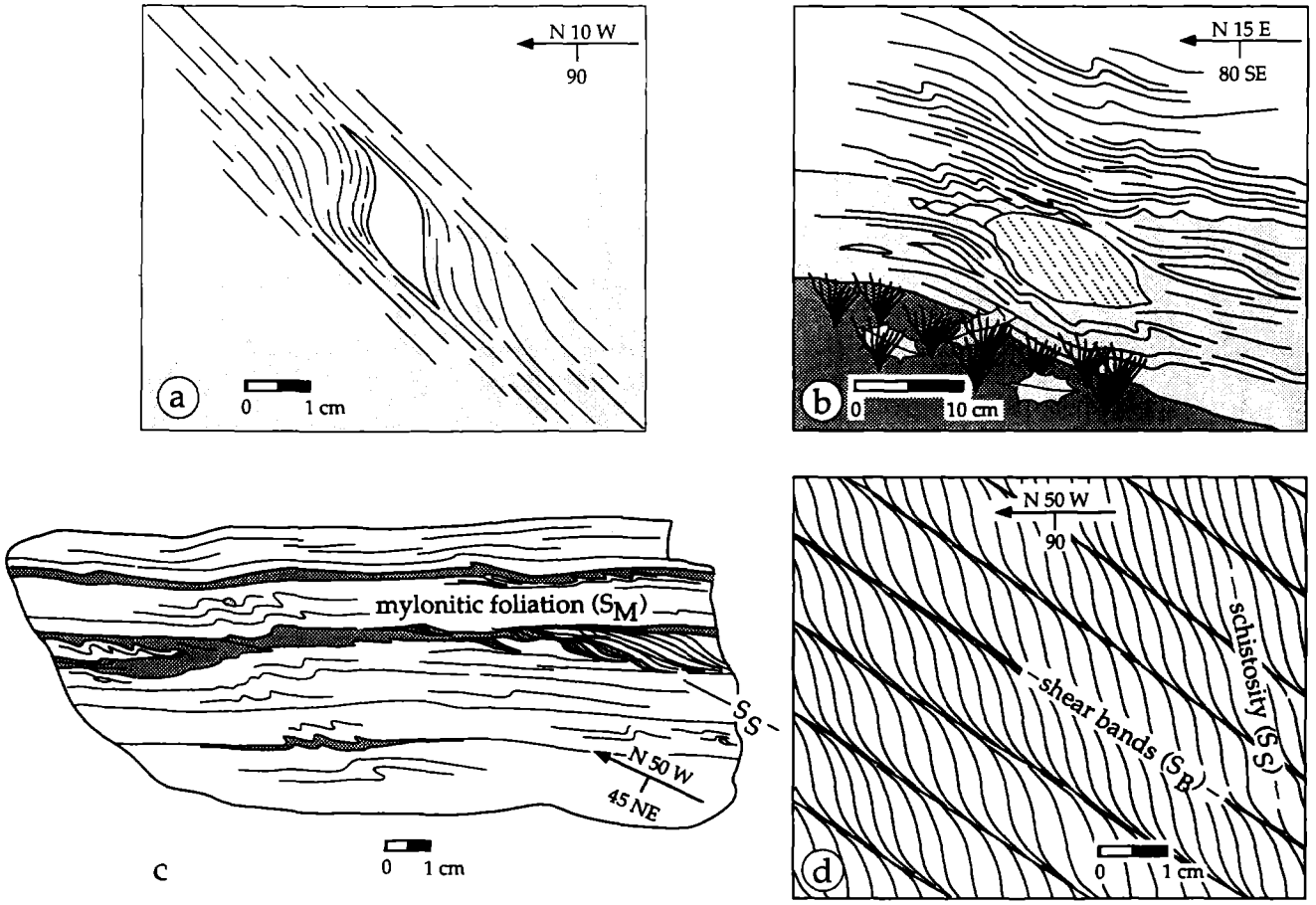

Fig. 3. Sketches of typical sense-of-shear criteria observed in the basement–Ashe boundary zone. (a) Porphyroclast with σ-type tails (south of Independence, VA). (b) Lens of less deformed granitic gneiss with σ-type geometry of tails (near Bina, NC). Note NW-vergent folds. (c) Partial tracing of fabric in slab of heterolithic mylonite showing NW-vergent folds and composite planar fabric (type II *S–C* of Lister & Snoke 1984) (near Newland, NC). (d) Composite planar fabric composed of shear bands and schistosity (Fries, VA). Although surfaces in (a) & (b) are oblique to the *XZ* section (perpendicular to foliation, parallel to stretching lineation), projected sense of shear is top-to-NW.

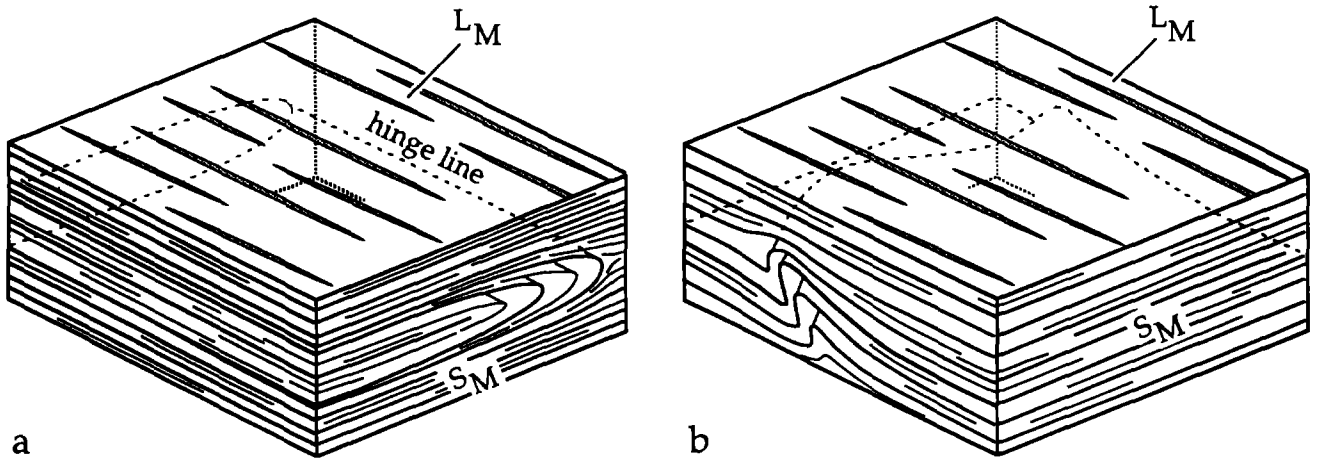

Fig. 4. Schematic illustrations of end-member fold geometries associated with fold hinge girdles. Folds are cm- to m-scale. (a) Isoclinal, cylindrical fold with attenuated limbs and a hinge line that is subparallel to stretching lineation. This geometry is most common among the folds observed in the basement–Ashe boundary zone. (b) Plane non-cylindrical fold with a hinge line that forms a high angle with stretching lineation. Folds of this geometry are NW-vergent.

Although few sheath folds were observed during the present study, hinge line data are consistent with a sheath geometry.

Planar dispersion of fold-hinge lines is evident in spherical projection (Fig. 2); hinge line data for segments de, fg, ij and jk are girdle-distributed through 180° and define planes that at first approximation are subparallel to mean mylonitic foliation. Hinge lines also show frequency maxima (T_3, Fig. 2) that closely coincide with the maxima in stretching lineations. Hinge lines that

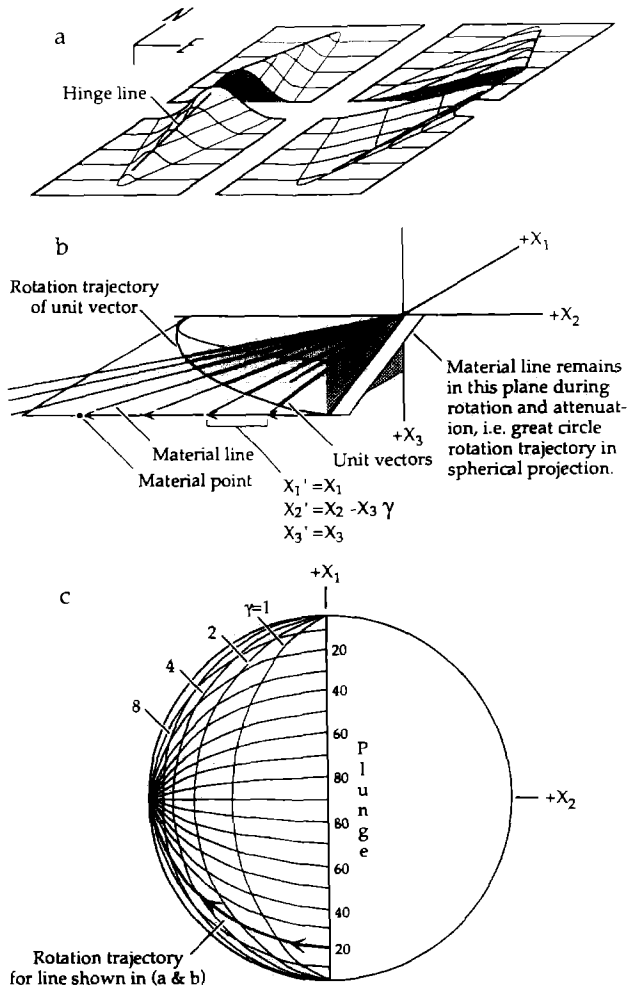

Fig. 5. Diagrams that illustrate the passive rotation of fold hinge lines in a top-to-E, horizontal, ductile shear zone. (a) Effect of top-to-E simple shear on a non-cylindrical buckle fold with a hinge line that initially lies perpendicular to the shear direction. (b) Rotation and stretch of a material line in the reference frame of the theoretical models. (c) Lower-hemisphere equal-area projection with contoured ($\gamma = 1$, 2, 4 and 8) great-circle rotation trajectories for lines that initially lie in the X_1X_3 plane (N–S trend, variable plunge).

define these maxima are associated with the isoclinal folds described above.

The related transitions of geometry and orientation of folds within a ductile shear zone, as presently described, suggest variable rotations of axes toward the extension direction and simultaneous modification of fold geometry, all due to progressive simple shear (Carreras *et al.* 1977) (Fig. 5a). The fact that S_M commonly defines these folds suggests a *contemporary* origin (i.e. shear related, Escher & Watterson 1974, see also Carreras *et al.* 1977, Evans & White 1984), as opposed to the possibility that the folds pre-date simple shear. Thus, it is suggested that folds in the basement–Ashe boundary zone nucleated continuously or at least periodically during thrusting and at a high angle to the extension direction, and that these folds were amplified, geometrically modified and rotated toward the extension direction by subsequent deformation. In this interpretation, isoclinal folds with hinge lines parallel to stretching lineation represent relatively early folds; open folds with hinge lines at a high angle to stretching lineation developed relatively late.

The structural data were analyzed statistically using the methods described by Cheeney (1983). Poles to mylonitic foliation and stretching lineations, which tend to be uniformly clustered about a mean, were analyzed using methods based on the Fisher vector distribution. Methods based on the Bingham axial distribution were used for hinge lines. These analyses reveal small and nearly constant angles (6° ± 1°) between the best-fit plane to hinge lines (plane of maximum and intermediate eigenvectors, T_3 and T_2, Fig. 2), and mean mylonitic foliation (calculated by vector addition of poles) (Table 1). Further, this 6° ± 1° angle can be formed in each case by incomplete top-to-W and top-to-NW rotation of the best-fit plane to hinge lines toward mean mylonitic foliation (Fig. 2). These observations inspired the theoretical model and analysis of previously published data.

Kinematic analysis

For kinematic analysis, it is assumed that: (1) the strain history resulting in mylonite below the Ashe Formation is dominated by simple shear: (2) mylonitic foliation (S_M) is either the shear plane or the flattening plane of finite strain and contains the intermediate strain axis in either case; and (3) mineral stretching lineation (L_M), of consistent NW–SE trend in the plane of S_M, is perpendicular to Y and represents either the shear direction or the X direction, depending on the interpretation of S_M. Figures 3 and 4(b) show rock fabric and mesoscopic structures that indicate non-coaxial deformation and top-to-NW sense-of-shear.

MODELS FOR PASSIVE ROTATION OF HINGE LINES IN SIMPLE SHEAR

Disregarding the fabric evidence for a contemporary origin, folds in the basement–Ashe boundary zone could be interpreted to pre-date simple shear deformation, in which case variable rotation and apparent geometric modification of the folds may reflect initial variability of orientation or inhomogeneous strain. Two cases, rotation of contemporary folds and rotation of pre-shear folds, have been modelled theoretically. These models (1 and 2, described below) were implemented using a microcomputer and the APL language. In subsequent text, each trial of either model is referred to as an *experiment*.

Both models employ a right-hand, orthogonal, Cartesian co-ordinate system in which $+X_1$ and $+X_2$ are horizontal and trend due N and due E, respectively, and $+X_3$ is 'down' (Fig. 5b). The modelled shear zone has a horizontal (X_1X_2) shear plane and an E–W (X_2) shear direction. Sense of shear was arbitrarily chosen as top-to-E. Passive rotation of a line element (hinge line) due to homogeneous simple shear is calculated by

Table 1. Statistical and geometric analyses of structural data from the basement–Ashe boundary zone. See Fig. 1 for segment locations and Fig. 2 for spherical projections

	segment de	segment fg	segment ij	segment jk
Mylonitic foliation (S_M)				
Mean pole (plunge trend)*	55 320	61 212	56 041	75 300
Length of mean pole†	0.95	0.96	0.95	0.94
Number of observations	63	26	22	17
0.90/0.95 confidence cones for mean pole (semi-apical angles)‡	3.6°/4.1°	5.2°/5.9°	6.1°/7.0°	7.2°/8.2°
Hinge lines				
T_1 (plunge trend, value)§	51 312, 0.39	64 225, 0.13	55 029, 0.58	70 300, 0.48
T_2 (plunge trend, value)§	17 200, 2.75	20 086, 2.94	21 266, 4.08	01 208, 4.55
T_3 (plunge trend, value)§	34 098, 9.86	16 350, 4.93	26 164, 11.34	20 118, 12.97
Number of observations	13	8	16	18
Fraction of variance explained by T_2 and T_3‖	0.97	0.98	0.96	0.97
0.90/0.95 confidence cones for T_1,¶ semi-apical angles measured in:				
T_1T_2 plane	17.2°/20.4°	13.6°/16.7°	14.7°/17.3°	11.4°/13.4°
T_1/T_3 plane	8.5°/10.0°	10.4°/12.7°	8.3°/9.8°	6.5°/7.6°
Mineral stretching lineation (L_M)				
Mean line (plunge trend)	31 108	02 312	11 318	15 124
Length of mean line	0.95	0.92	0.94	0.92
Number of observations	146	25	20	18
0.90/0.95 confidence cones for mean line (semi-apical angles)	2.3°/2.6°	7.3°/8.4°	6.8°/7.7°	8.7°/9.9°
Geometric analysis				
'Calculated shear direction' (plunge trend)**	20 081	15 330	02 134	15 120
Sense-of-shear††	Top-to-W	Top-to-NW	Top-to-NW	Top-to-NW
Angle between mean L_M and calculated shear direction	26°	22°	14°	4°
Angle between mean pole to S_M and T_1 for hinge lines	6°	7°	7°	5°

*Mean poles and mean lines were calculated by vector addition. Plunge and trend values are given in degrees.

†Length of mean pole and mean line is a measure of concentration about the mean that ranges in value from 0 to 1. Spherical variance (Mardia 1972, p. 219) is given by 1-length.

‡Confidence cones for mean pole and mean line were calcualted by the Fisher approximations given by Cheeney (1983, equation 9.7).

§T_1, T_2 and T_3 refer to the three eigenvectors following the convention, $t_1 < t_2 < t_3$ (t is the eigenvalue).

‖Fraction of variance explained by T_2 and T_3 was calculated as $(t_2 + t_3)$/number of observations. A good fit of the data to a plane is indicated by $t_1 \lll t_2 \leq t_3$ and a "fraction of variance explained by T_2 and T_3" close to 1. The best-fit plane (BFP) to hinge lines is the T_2T_3 plane, for which T_1 is the pole.

¶Confidence cones for T_1 were calculated by the Bingham approximations given by Cheeney (1983, equation 9.12).

**The 'calculated shear direction' is the line in the plane of mean mylonitic foliation that is normal to the intersection of the BFP to hinge lines and mean mylonitic foliation.

††Sense-of-shear was interpreted from incomplete rotation of the BFP to hinge lines toward mean mylonitic foliation.

$$\begin{bmatrix} X_1' \\ X_2' \\ X_3' \end{bmatrix} \quad \begin{bmatrix} 1 & 0 & 0 \\ 0 & 1 & -\gamma \\ 0 & 0 & 1 \end{bmatrix} \quad \begin{bmatrix} X_1 \\ X_2 \\ X_3 \end{bmatrix},$$

where X_1, X_2 and X_3 are direction cosines for the tip of a unit vector that represents a hinge line and X_1', X_2' and X_3' are co-ordinates for the tip of the same vector after rotation and stretch due to a simple shear of γ (Fig. 5b). Shear strain is negative in the transformation matrix so that top-to-E angular shear, Ψ, and shear strain, γ, can be considered positive in the reference frame of the models.

Model 1

Model 1 simulates passive rotation of contemporary folds. In these experiments, the simple shear transformation was applied repeatedly with $\gamma = 0.25$ to a matrix of hinge lines, such that shear strain accumulated incrementally to the chosen limit for each experiment ($6 \leq \gamma \leq 50$). Incremental accumulation of shear strain is unnecessary but approximates a continuous deformation, an important concept of the present model. At the start of each experiment, the hinge line matrix contained a single hinge line. A new hinge line was introduced to the modelled shear zone (added to the hinge line matrix) at intervals of $\gamma = 0.5$, 1 and 2 in separate sets of experiments. The rate of fold nucleation was varied to test the sensitivity of the results to this variable. Actual rates of fold nucleation in ductile shear zones have not been established and probably vary widely. Hinge lines were randomly selected from normally distributed populations described in Table 2. Figure 6 shows a sample from each initial population ($n = 50$) in spherical projection. The centers of populations A, B and C lie in the shear plane and are

Table 2. Model populations

Model population	Center of distribution (plunge/trend)	Standard deviations	
		plunge	trend
A	0/180	15°	5°
B	0/180	10°	30°
C	0/180	10°	60°
D	15/165	10°	10°
E	random	—	—

perpendicular to the shear direction. This is the approximate orientation in which contemporary folds presumably form (Escher & Watterson 1974, Williams 1978, Butler 1982), plausibly as non-cylindrical buckles (Rhodes & Gayer 1977, Ghosh & Sengupta 1984, 1987). The center of population D is oblique to both the XZ plane and the shear plane. This may be the case, for example, if folds develop in a competent layer other than mylonitic foliation. The random population (E) portrays no specific situation and was used to check further the dependency of the model on the choice of initial fold orientation. As Anderson (1976) pointed out, the distribution of such populations (normal or otherwise) is irrelevant, as long as selection from them is random. Normal distributions were chosen for computational convenience.

Results. Hinge lines at the conclusion of each experiment using model 1 provided a good fit to a plane; examples are shown in Fig. 7. In every case, 93–99% of the total variance was explained by the intermediate (T_2) and maximum (T_3) eigenvectors ($[(t_2 + t_3)/n] \times 100$, where t is the eigenvalue). In experiments based on population E, resulting distributions were markedly clustered with 70–90% of the total variance explained by T_3 alone ($((t_3/n) \times 100)$. High strain experiments ($\gamma \geq 10$) based on populations A–D resulted in more complete girdle distributions. Separation angles (Hansen 1971) are most apparent in experiments based on populations A and B, and become progressively smaller as shear strain is increased.

Rotation of the best-fit plane (BFP) to hinge lines (T_2T_3 plane) towards the shear plane was always incomplete in model 1, leaving a small angle (β) between these planes (Fig. 8). Similarly, a small angle (θ') lies between the XY plane of the finite strain ellipsoid and the shear plane (Fig. 8, see also Ramsay & Huber 1983). In high strain experiments, β was always larger than θ'; differences ($\beta - \theta'$) of 2–5° were found in experiments based on populations A, B and C, 3–10° in experiments based on population D, and as large as 60° in experiments based on population E. Several low-strain experiments based on populations B and C resulted in β smaller than θ', due to the initial dispersion of the hinge lines in the shear plane (Fig. 6).

As shown by model 1, variable rotation of contemporary folds resulting in a planar dispersion of hinge lines can be attributed to (1) variable inclination of hinge lines with respect to the shear plane, which affects the rate of rotation (Fig. 5c) and (2) sequential fold development during progressive simple shear, such that folds are affected by different values of shear strain.

Model 2

Model 2 simulates passive rotation of folds that predate shear. In these experiments, rotation of hinge lines was calculated in a single step, rather than incrementally, as in model 1. The hinge line matrix was loaded at the start of each experiment and each hinge line had the same shear strain applied to it. Hinge lines were randomly selected from the same populations specified for model 1. Although these populations are rather arbitrary for model 2, using them allows direct comparison of the results.

Results. In all variants of model 2, hinge lines become dispersed in the XY plane at $\gamma > 10$ (Figs. 8 and 9). Only in low strain experiments based on populations B and C, is the BFP to hinge lines significantly different (closer to the shear plane) than the XY plane. As for similar results of model 1, this can be attributed to the initial dispersion of populations B and C in the shear plane (Fig. 6). Also as for model 1, separation angles are apparent in experiments based on populations A and B and become progressively smaller as strain is increased. Results of model 2 are different from those of model 1 in two respects. (1) For any given shear strain, rotation of the BFP to hinge lines is advanced as compared to model 1. (2) Patterns resulting from model 2 experiments at high strains show a higher point density subparallel to the shear direction (Fig. 9). Similar patterns were illustrated by Skjernaa (1980) for comparable experiments in which different initial fold populations were used. In model 2, variable rotation of hinge lines resulting in a planar distribution can only be due to differences in inclination of hinge lines with respect to the shear plane and the effect that this has on the rate of rotation (Fig. 5c).

NATURAL FOLD-HINGE GIRDLES

The Blue Ridge thrust complex, southern Appalachians

Remarkably constant angles of 6° ± 1° between the best-fit plane (BFP) to hinge lines and mean mylonitic foliation occur in four segments of the basement–Ashe boundary zone, spanning more than 100 km of the boundary length (Table 1 and Fig. 2). Each 6° ± 1° angle can be formed by incomplete top-to-W and top-to-NW rotation of the fold-hinge girdle toward mean mylonitic foliation, the sense of shear also indicated by independent kinematic analysis. This suggests that sense of shear can be determined from the geometric relationship of the fold-hinge girdle to mylonitic foliation. Depending upon how mylonitic foliation is interpreted, incomplete rotation of the BFP to hinge lines can be explained by either of the theoretical models, rotation of contemporary folds (model 1) or of pre-shear folds (model 2). However, folds of mylonitic foliation define the fold-

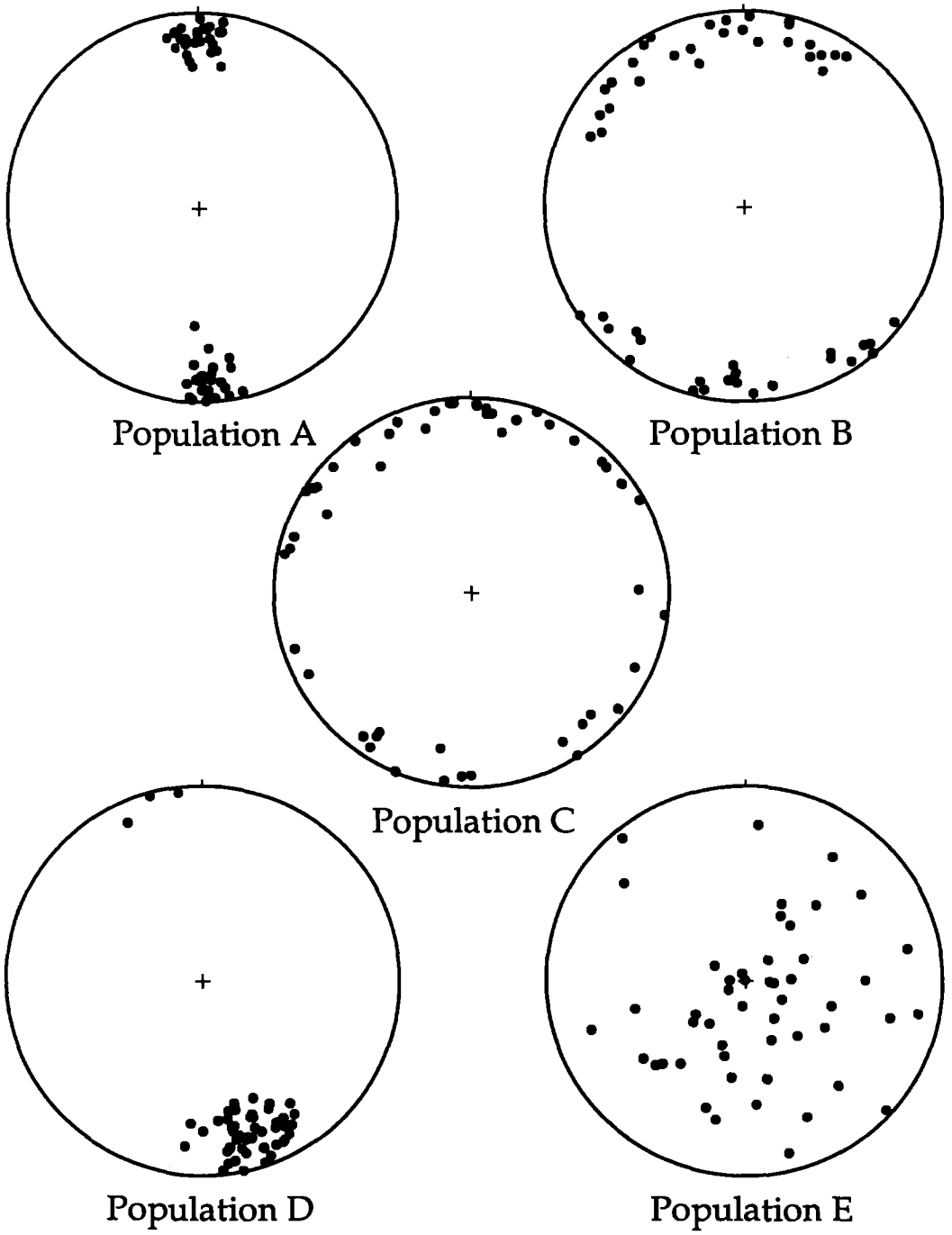

Fig. 6. Lower-hemisphere equal-area projections of randomly selected initial hinge lines (n = 50) from model populations A–E. Populations are described in Table 2.

hinge girdles, suggesting a contemporary origin (i.e. model 1). Applications of the theoretical models with different interpretations of mylonitic foliation are given in the discussion.

Other areas

To substantiate the kinematic interpretation of fold-hinge girdles, previously published data were also analyzed. The analysis requires data for mylonitic foliation and stretching lineation, as well as data that define the fold-hinge girdle. Documentation of the necessary data was the only criterion used in the selection of case studies. No filters were applied during the selection and all cases analyzed are reported. Because structural data must be quantitative and are generally published only in spherical projection, these projections were digitized and trend and plunge were recovered from them.

Data from previous reports are totally independent of ideas expressed in this paper and, therefore, provide the best possible test of them. These tests are, however, somewhat contingent on interpretation by the original geologist during data collection and may include error inherent in the graphical representation of the published data.

Eight data sets from six papers have been analyzed (Table 3 and Fig. 10). In each case, independent evalu-

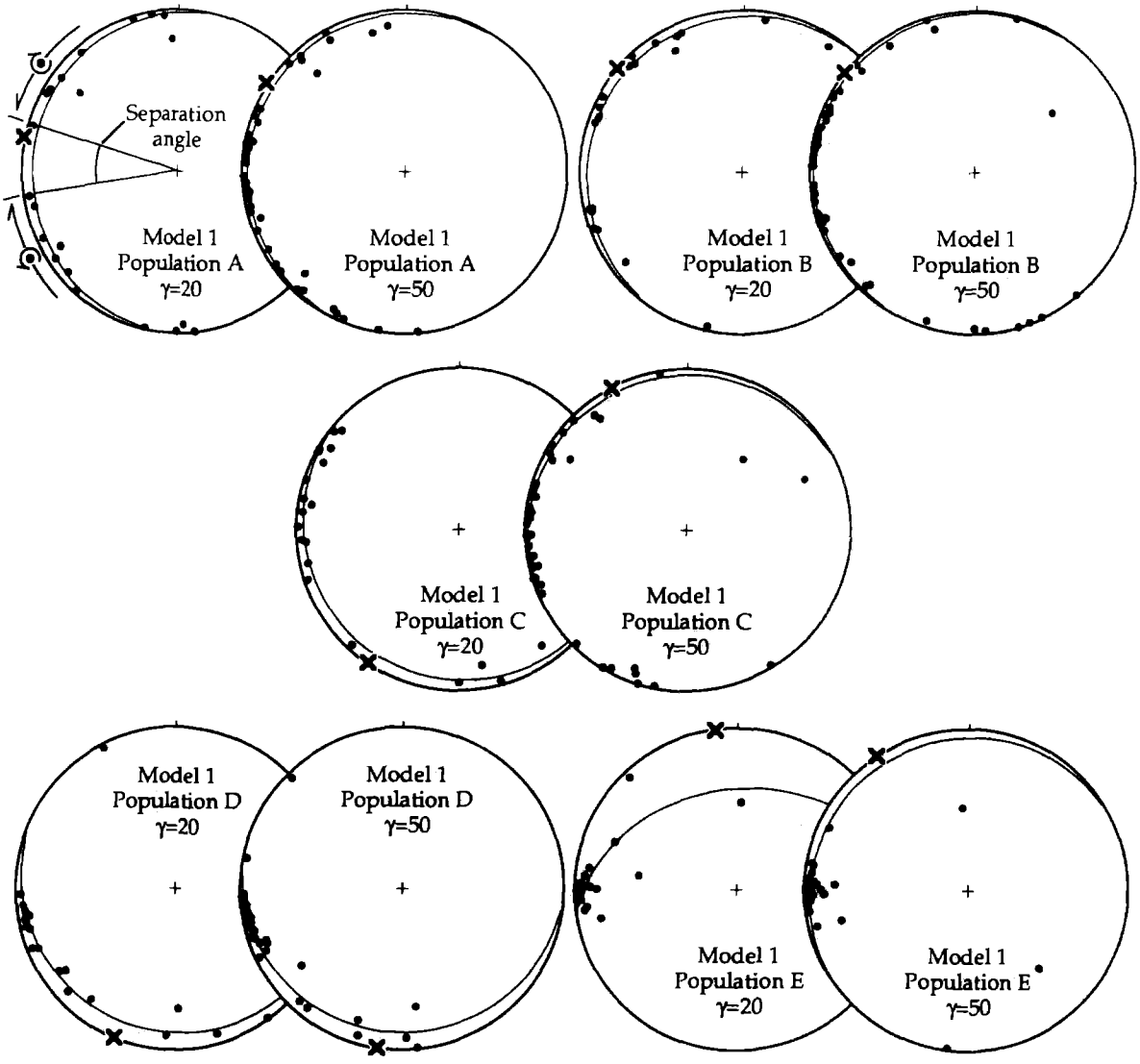

Fig. 7. Results of model 1 (contemporary folds) experiments shown in lower-hemisphere equal-area projections. In each case, hinge lines were added to the model at the rate of $1/1\gamma$. Great circles are best-fit planes (BFPs) to hinge lines, the incomplete rotation of which reflects top-to-E simple shear. xs are shear directions calculated as the line in the shear plane that is normal to the intersection of the BFP to hinge lines and the shear plane (see discussion). The actual shear direction is horizontal E–W. The separation angle and fold rotation sense is shown in the upper-left diagram.

ation of sense of shear was used to check the kinematic interpretation of the fold-hinge girdle.

The Variscan nappes

Vauchez *et al.* (1987) described a subhorizontal shear zone below the Variscan nappes in South Brittany, France, and contemporary folds in and adjacent to the shear zone. Their kinematic analysis indicates top-to-W displacement.

Vauchez *et al.* (1987) provided two data sets, one from the hanging wall (porphyroids) and the other from the footwall (Silurian basement). The hanging wall data include an isolated cluster of three stretching lineations and four hinge lines that were discounted in the present analysis. These data are inconsistent with patterns clearly defined by the majority of the data in this set (nine stretching lineations, 23 hinge lines). Analyses of the remaining data indicate angles of 22° and 34° between mean mylonitic foliation and fold-hinge girdles for the hanging wall and footwall, respectively, and top-to-SW vergence in each case (Figs. 10a & b).

Vauchez *et al.* (1987) considered the hinge lines to be scattered within the mean plane of mylonitic foliation. In the present analysis, moderate angles between the BFP to hinge lines and mean mylonitic foliation and between the 95% confidence cones for poles to these planes were determined.

The Moine thrust

Comprehensive structural data for the Moine thrust in the Assynt region of Scotland were given by Christie (1963). Stretching lineations in this area plunge gently to the east, roughly down-dip, in the plane of mylonitic foliation. Kinematic analysis of Butler (1982), Evans & White (1984) and Law *et al.* (1986) indicated top-to-NW

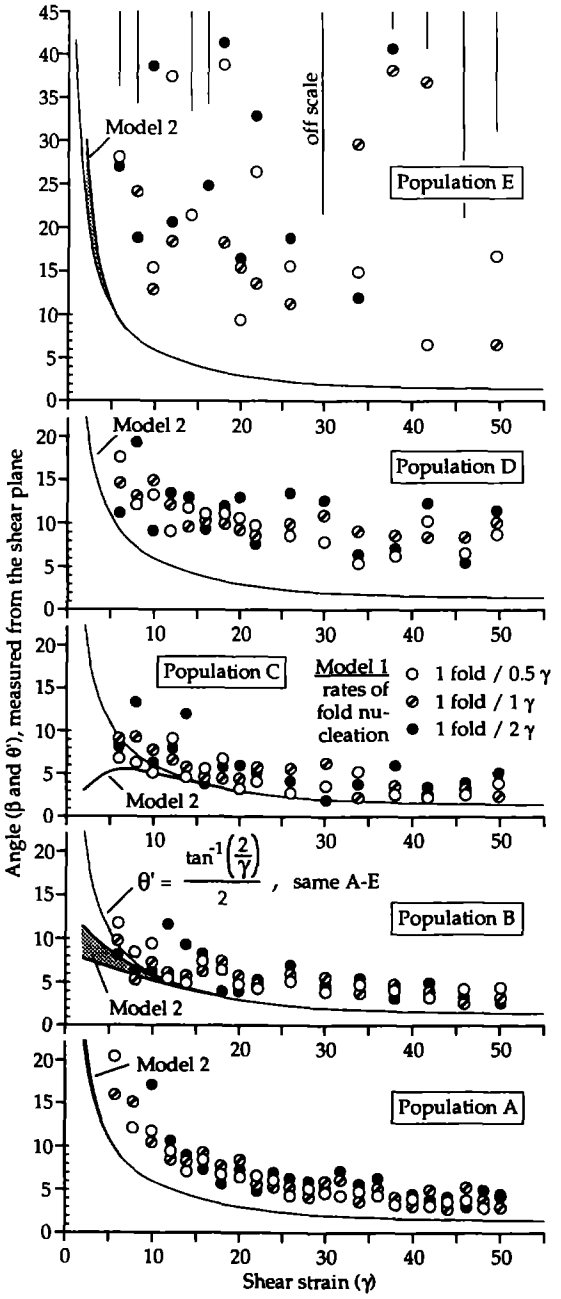

Fig. 8. Plots of shear strain against β and θ'. Results of model 1 experiments with different rates of fold nucleation are plotted as circles (see legend with graph for population C). Model 2 experiments were repeated 3 times for each value of γ (γ = 6, 8, 10, . . . 50). The resulting envelopes (population B, $\gamma < 10$, for example) are due to random selection of hinge lines from model populations. See text for further explanation.

and top-to-W displacement in the Assynt region and areas to the north.

Butler (1982) described minor folds associated with the Moine thrust south of Loch Eriboll, 25 km north of Assynt. These are folds of mylonitic fabric with NE–SW trend that refold NW-trending intrafolial isoclines. Following Escher & Watterson (1974), Butler (1982) considered these to be contemporary folds. Fold-hinge girdles defined by Christie's (1963) data are consistent with this hypothesis.

Analyses of Christie's (1963) data indicate angles of 4° and 6° between mean mylonitic foliation and fold-hinge girdles for the Stack of Glencoul and Cnoc a' Chaoruinn areas, and top-to-NW and top-to-SW senses, respectively (Figs. 10c & d).

Honey Hill mylonite zone

In the case of the Honey Hill mylonite zone in Connecticut, U.S.A., Goldstein (1988)* provided both orientation and vergence data for girdle-distributed intrafolial folds. A separation angle (Hansen 1971) separates folds of 'S' and 'Z' asymmetries. The bisector of the separation angle lies approximately parallel to stretching lineation, which plunges gently to the NW. Goldstein's (1988) kinematic analysis indicates low-angle normal displacement (top-to-NW).

The angle between mean mylonitic foliation and the fold-hinge girdle in this case is 8°, and the sense of displacement interpreted from this relationship is top-to-W (Fig. 10e).

The South Armorican shear zone

An anomalous northward dipping (20–40°) mylonite zone occurs within the South Armorican shear zone of western France, which is otherwise subvertical (Jegouzo 1980). Non-cylindrical folds in ultramylonite from this zone have been described by Jegouzo and structural data, including a fold-hinge girdle, are shown in his fig. 5. Stretching lineation in the anomalous zone is subhorizontal with E–W trend and sense of shear criteria indicate a dextral shear component (Jegouzo 1980), as previously determined by Berthé *et al.* (1979).

In this case, the angle between mean mylonitic foliation and the fold-hinge girdle is 17°, and a dextral (top-to-SE) sense is indicated (Fig. 10f).

Muscat nappes

Michard *et al.* (1984) described folds, some of which are non-cylindrical, from the Muscat nappes in Oman. The fold-hinges define a girdle and a separation angle. The principal rock fabric here is not described specifically as mylonitic, but rather as a penetrative cleavage that transposes an earlier foliation. It is interpreted as due to strain with a SSW-directed simple shear component. Planar dispersion and noncylindricity of folds is also attributed to simple shear (Michard *et al.* 1984).

Analysis of the Muscat nappe data indicates an angle of 32° between the fold-hinge girdle and mean mylonitic foliation, and top-to-S displacement (Fig. 10g). Myloni-

*The author regrets an error in the present treatment of Goldstein's (1988) hinge line data that propagated through the statistical and geometric analysis. Analysis of the corrected data indicates a 6° angle between mean mylonitic foliation and the best-fit plane to hinge lines, and closer agreement (18°) between mean stretching lineation and the 'calculated shear direction'. The sense of shear indicated by the geometric analysis (top-to-W) is unchanged.

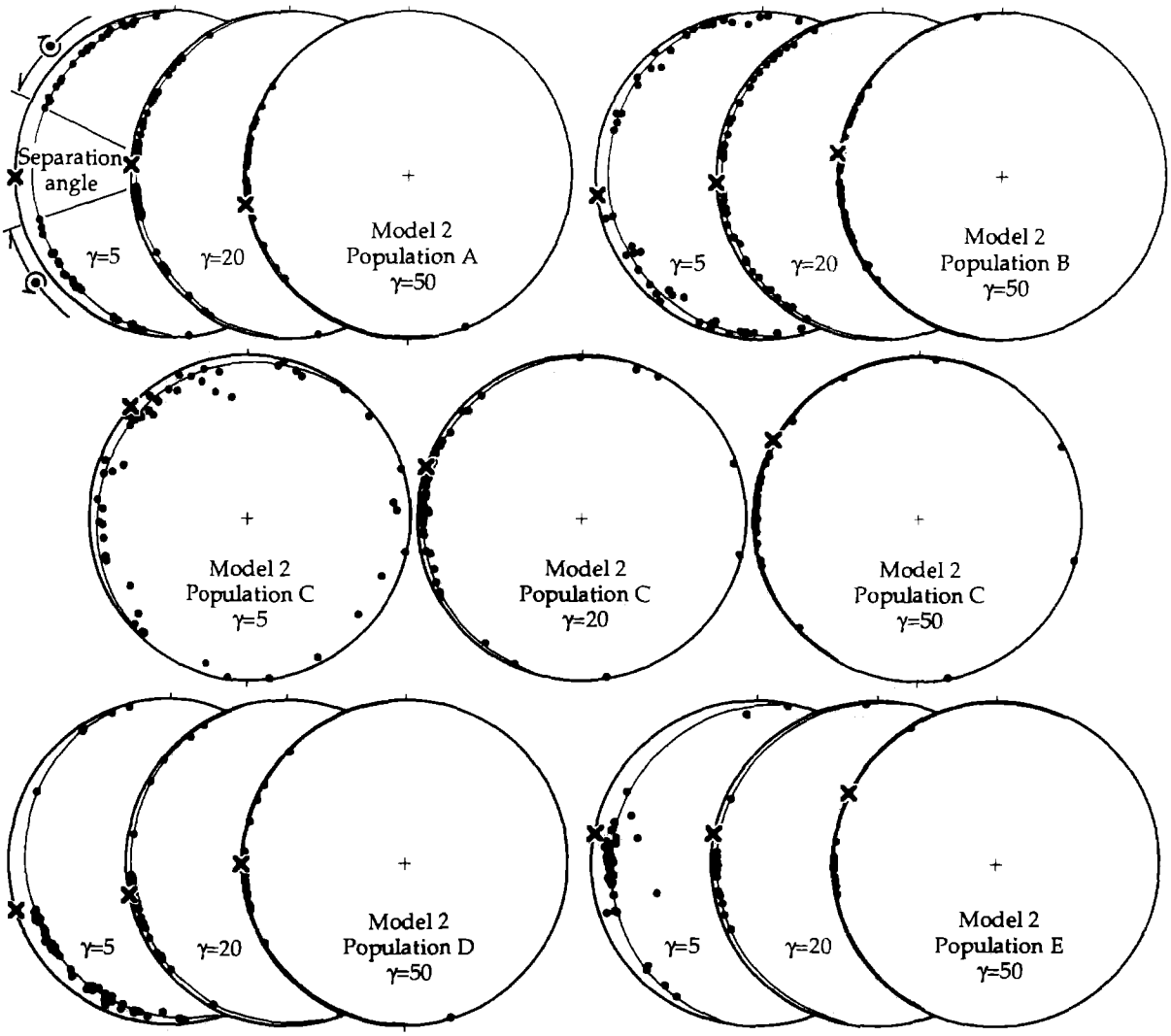

Fig. 9. Results of model (pre-shear folds) experiments shown in lower-hemisphere equal-area projections. Great circles and **x**s as in Fig. 7. The shear direction is horizontal E–W, as for model 1.

tic foliation and the fold-hinge girdle are not coplanar, as Michard *et al.* suggested.

Cap de Creus shear zones

Carreras *et al.* (1977) provided an excellent description of contemporary folds in Cap de Creus quartz-mylonites, northeast Spain. These folds deform mylonitic foliation, are commonly non-cylindrical (sheath folds) and define a fold-hinge girdle (steep NE dip) with a concentration of hinge lines parallel to stretching lineation (gentle NW plunge). Vergence of folds that plunge to the NE, at a high angle to stretching lineation, is clockwise (viewed down-plunge), indicating top-to-SE (dextral) displacement. The opposing vergence of folds that lie subparallel to stretching lineation suggests a closed separation angle. Detailed analysis of fold geometry, style, and orientation, and of crystallographic fabric led Carreras *et al.* to the contemporary fold interpretation.

The hinge line data for the Cap de Creus mylonites define a plane that is incompletely rotated into mylonitic foliation, leaving an angle of 9° (present analysis). Top-to-S (dextral) displacement is indicated (Fig. 10h).

DISCUSSION

Initiation of folds in ductile shear zones

As Ghosh & Sengupta (1987) pointed out, a problem with the initiation of folds in shear zones, particularly at high angles to stretching lineation, is to explain how mylonitic foliation, approximately (or precisely) parallel to the *XY* plane, is folded. The phenomenon is equally odd when viewed in light of a simple card deck experiment which demonstrates that the shear plane in perfect simple shear, a possible interpretation of mylonitic foliation, is a plane of no finite longitudinal strain (Ramsay & Huber 1983). Rhodes & Gayer (1977) suggested that layer-parallel compression resulting in buckle folds at a high angle to stretching lineation can develop during layer-parallel shear between areas of relatively high interlayer cohesion. A similar model was presented by Ghosh & Sengupta (1984, 1987) and is the basis for model fold populations A, B and C used in the present paper. Alternatively, mechanical instability caused by the deflection of foliation around objects such as elliptical pods or boudin segments can cause the generation of

Table 3. Statistical and geometric analyses of structural data from previous reports. See Fig. 10 for spherical projections.

	Variscan nappes, South Brittany, France		Moine thrust, Assynt Region, Scotland		Honey Hill mylonite zone, Connecticut, U.S.A.‖	South Armorican shear zone, France¶	Muscat nappes, Oman**	Cap de Creus shear zones, Spain††
	Porphyroids*	Silurian basement†	Stack of Glencoul‡	Cnoc a' Chaoruinn§				
Mylonitic foliation (S_M)								
Mean pole (plunge trend)	67 223	75 229	71 243	68 300	67 116	73 183	81 120	44 242
Length of mean pole	0.93	0.96	0.97	0.97	0.98	0.95	0.96	0.98
Number of observations	80	75	34	20	20	12	10	15
0.90/0.95 confidence cones for mean pole (semi-apical angles)	4.2°/3.7°	2.9°/3.3°	3.9°/4.5°	4.9°/5.6°	3.8°/4.4°	7.9°/9.0°	8.4°/9.5°	4.8°/5.5°
Hinge lines								
T_1 (plunge trend, value)	45 220, 0.64	41 235, 0.40	69 252 1.95	66 284, 3.03	75 127, 0.31	57 169, 0.22	53 170, 0.09	37 235, 0.86
T_2 (plunge trend, value)	17 327, 5.92	20 127, 6.05	05 356, 38.46	08 032, 28.25	02 030, 5.66	30 017, 1.97	01 262, 3.48	52 036, 15.80
T_3 (plunge trend, value)	40 073, 16.44	43 017, 9.54	20 088, 61.60	23 126, 94.72	15 300, 9.03	13 280, 6.81	37 353, 4.43	09 138, 37.34
Number of observations	23	16	101	123	15	9	8	54
Fraction of variance explained by T_2 and T_3	0.97	0.97	0.98	0.98	0.98	0.97	0.99	0.98
0.90/0.95 confidence cones for T_1, semi-apical angles measured in:								
T_1T_2 plane	9.9°/11.6°	9.6°/11.3°	2.9°/3.3°	3.9°/4.4°	9.0°/10.5°	19.9°/24.2°	10.0°/12.3°	4.2°/4.8°
T_1T_3 plane	5.7°/6.6°	7.5°/8.8°	2.2°/2.6°	2.0°/2.3°	7.0°/8.2°	10.1°/12.2°	8.9°/10.9°	2.7°/3.1°
Mineral stretching lineation (L_M)								
Mean line (plunge trend)	33 095	13 085	17 103	21 100	19 309	14 275	11 018	13 342
Length of mean line	0.97	0.89	0.99	0.98	0.98	0.98	0.88	0.99
Number of observations	9	23	67	69	22	5	7	7
0.90/0.95 confidence cones for mean line (semi-apical angles)	7.1°/8.2°	8.7°/9.9°	1.8°/2.1°	2.3°/2.7°	3.3°/3.8°	7.3°/8.3°	17.4/19.9°	4.8°/5.5°
Geometric analysis								
'Calculated shear direction' (plunge trend)	23 035	14 047	06 135	06 046	22 277	15 336	04 001	33 011
Sense of shear	Top-to-SW	Top-to-SW	Top-to-NW	Top-to-SW	Top-to-W	Top-to-SE (dextral)	Top-to-S	Top-to-S (dextral)
Angle between mean L_M and calculated shear direction	53°	37°	33°	54°	30°	59°	18°	35°
Angle between mean pole to S_M and T_1 for hinge lines	22°	34°	4°	6°	8°	17°	32°	9°

Explanation as for Table 1.
Sources of data: *Vauchez *et al.* (1987, fig. 5a); †Vauchez *et al.* (1987, fig. 5b); ‡Christie (1963, figs 5 and 6); §Christie (1963, figs. 11 and 12); ‖Goldstein (1988, fig. 3); ¶Jegouzo (1980, fig. 5); **Michard *et al.* (1984, fig. 15); ††Carreras *et al.* (1977, fig. 4).

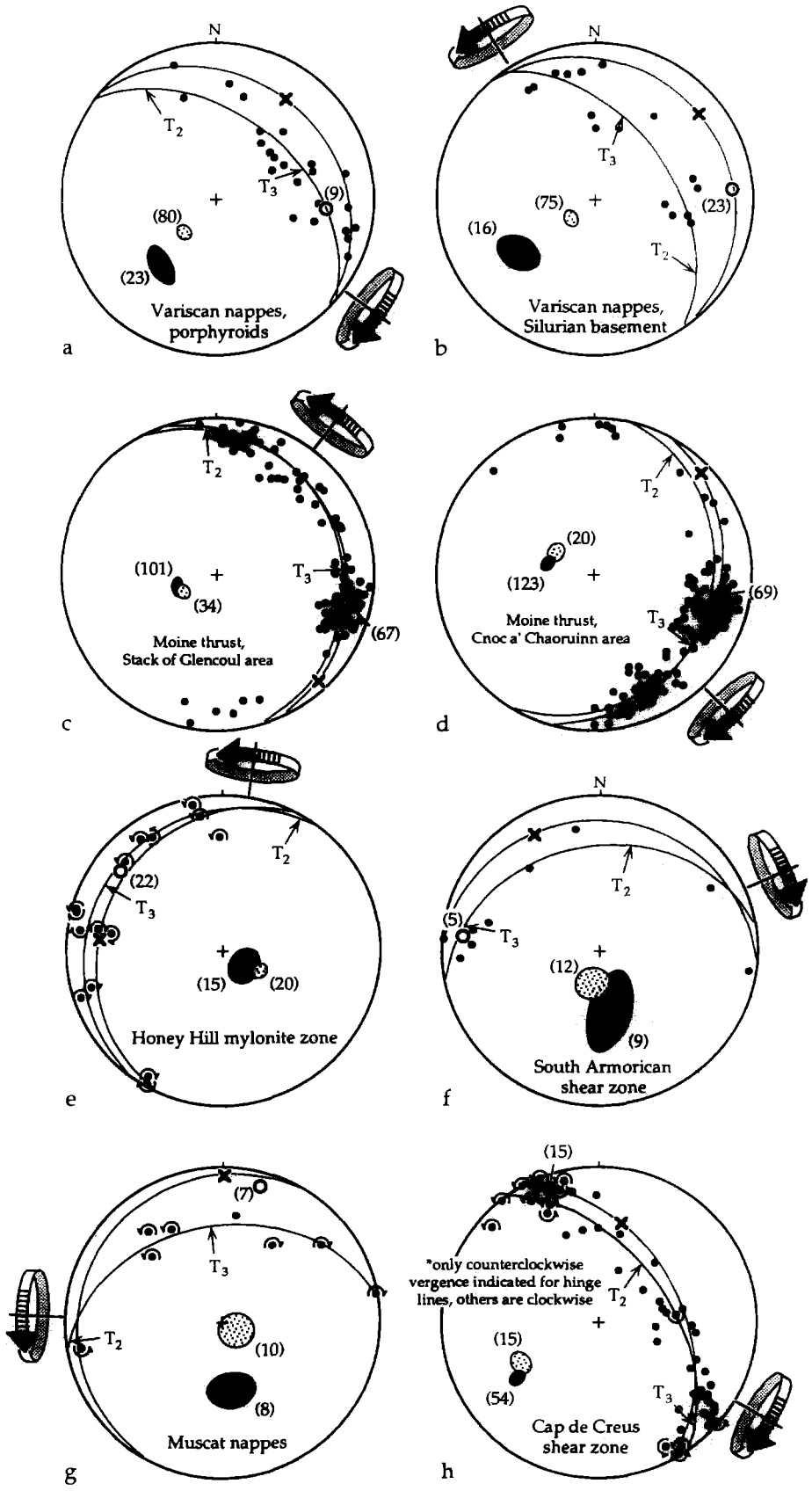

Fig. 10. Lower-hemisphere equal-area projections of fold hinge girdles from previous reports with statistical and geometric analyses of the present paper (see Table 3). 95% confidence cones for minimum eigenvectors are shaded. Other symbols are as shown in Fig. 2. For clarity, mylonitic foliation and stretching lineation data are represented only by statistical parameters (i.e. 95% confidence cone for mean pole to mylonitic foliation, stippled, and mean stretching lineation, bold open circle). Fold rotation sense (viewed down plunge) is shown for the Honey Hill mylonite zone, the Muscat nappes and the Cap de Creus shear zones. Data are from the following sources: (a) & (b) Vauchez *et al.* (1987, figs. 5a & b); (c) & (d) Christie (1963, figs. 5, 6, 11 and 12); (e) Goldstein (1988, fig. 3); (f) Jegouzo (1980, fig. 5); (g) Michard *et al.* (1984, fig. 15); and (h) Carreras *et al.* (1977, fig. 4).

folds, due either to passive flow (e.g. Cobbold & Quinquis 1980) or to active folding of mylonitic foliation that locally lies in the bulk shortening field (Bell & Hammond 1984, Fossen & Rykkelid 1990). However, as Platt (1983) pointed out and as is true of the basement–Ashe boundary zone, most shear zone folds are not associated with 'islands' of less deformed rock.

It is interpreted in the present paper, as it was in others (e.g. Bryant & Reed 1969, Bell 1978, Evans & White 1984), that hinge lines of contemporary folds are rotated toward parallelism with stretching lineation from an initially high angle (model populations A, B and C). However, relatively open folds of mylonitic foliation with axes approximately parallel to stretching lineation have been described from other areas (e.g. Bell & Hammond 1984, Ghosh & Sengupta 1987). Because these folds lack the isoclinal form of rotated folds, they have been interpreted as having initiated subparallel to stretching lineation. In the present case of the basement–Ashe boundary zone, the planar dispersion of hinge lines and the associated fold geometries suggest that variable rotation of hinge lines toward stretching lineation has occurred; open folds that lie subparallel to stretching lineation have not been observed.

Application of the models

In the case that mylonitic foliation is the XY plane of the finite strain ellipsoid, only model 1 can explain incomplete rotation of the best-fit plane (BFP) to hinge lines toward mean mylonitic foliation. In model 2, the two planes become one and the same at $\gamma > 10$ (see *Results*, *Model* 2). By direct application of model 1 with model populations A, B or C and with the premise that mylonitic foliation is the XY plane, the 4–9° angle common to eight of the 12 natural test cases ($\beta - \theta'$ in Fig. 8) suggests shear strains (γ) as large as 40. However, the moderate angles (17–34°) determined for the Variscan nappes, the Muscat nappes, and the South Armorican shear zone are not predicted by model 1 (except for random experiments based on population E). This deficiency of the model is improved (but is not overcome) if folds do not begin to form until after mylonitic foliation is well developed (Carreras *et al.* 1977, p. 13). In this case, rotation of mylonitic foliation, as the XY plane, is ongoing from the earliest history of the shear zone and is therefore advanced before the fold-hinge girdle develops. Thus, β angles plotted in Fig. 8 are displaced toward higher shear strain, such that the difference between β and θ' is increased for a given value of γ (and values of γ that correspond to the 4–9° angle are also increased).

In the case that mylonitic foliation is the shear plane, either model may explain incomplete rotation of the fold-hinge girdle. However, model 1 may better explain the constancy of the angle observed between the BFP to hinge lines and mean mylonitic foliation. As shown in Fig. 8, rotation of the BFP to hinge lines is retarded by continuous addition of contemporary folds. For model 1 with model populations A, B or C, β is nearly constant and has a value between 4° and 9° for a wide range of γ ($10 \leq \gamma \leq 50$). Conversely, curves for model 2 in Fig. 8 relate the 4–9° angle to a narrower range of γ ($7 \leq \gamma \leq 20$), which is unlikely to reflect actual shear strain in so many different shear zones. Further, large shear strains are suggested by near parallelism of hinge lines and stretching lineation (cf. Skernaa 1980). Assuming that hinge lines of contemporary folds initially lie at a high angle to the shear direction (Escher & Watterson 1974, Williams 1978, Butler 1982, Ghosh & Sengupta 1984) and are inclined no more than 15° relative to the shear plane, $\gamma \geq 10$ is required to rotate hinge lines to within 30° of stretching lineation; $\gamma > 20$ is required to reduce this angle to 10° (Fig. 5c), which is significantly larger than many observations of this angle. For these reasons and because contemporary folds are commonly decribed from ductile shear zones (e.g. Escher & Watterson 1974, Butler 1982, this paper), model 1, with the shear plane interpretation of mylonitic foliation, is favored.

The common value of 4–9° between the BFP to hinge lines and mean mylonitic foliation may have an alternative explanation. Early folds in the contemporary fold model (model 1) may be attenuated beyond recognition at some shear strain (γ_r) and may thus be effectively removed from the cumulative hinge line population, erasing the record of early strain in the fold system and resulting in a steady-state value of β for $\gamma > \gamma_r$. In the natural analogue, this is expressed as an unavoidable bias in hinge line data; more completely rotated (and attenuated) hinge lines that would normally pull the BFP toward mean mylonitic foliation are not recognized. In this scenario, which may apply with either interpretation of mylonitic foliation considered above, rotation of the fold-hinge girdle is suspended at β (or $\beta - \theta'$) = 4–9°.

Four of the 12 test cases show moderate angles between the BFP to hinge lines and mean mylonitic foliation (Table 3 and Fig. 10). The larger three of these values (17, 22, 32 and 34°) are associated with nappes (Muscat and Variscan) and may reflect lower shear strain common to nappes. If either model (1 or 2) with either interpretation of mylonitic foliation (shear plane or XY plane) portrays these cases, $\gamma < 5$ is indicated (Fig. 8) and rotation of hinge lines toward the shear direction should be incomplete (Fig. 5c), resulting in a relatively wide separation angle (Hansen 1971). However, the data include hinge lines that are subparallel to stretching lineation (Fig. 10), which requires shear strains considerably larger than 5 if these hinge lines have been rotated through a large angle (Fig. 5c). This is recognized as an inconsistency with the present models that may be ameliorated if some of the folds in these cases had initiated at a low angle to the extension direction (Bell & Hammond 1984, Ghosh & Sengupta 1987), as is provided by model population C. In test cases that yield moderate angles, mean mylonitic foliation and the BFP to hinge lines are distinct, even at high (99%) degrees of confidence (based on Fisher and Bingham distributions). In these cases, as in the others,

the general geometric relationship between these planes provides sense of shear.

Theoretically, if hinge lines in the modelled shear zone were distributed symmetrically about the XZ plane, the Y direction (X_1 in the models) would be defined by the intersection of the best-fit plane to hinge lines with the shear plane, and the shear direction would lie in the shear plane, perpendicular to this intersection. 'Calculated shear directions' determined in this way are reported in Tables 1 and 3 and are shown in Figs. 2, 7, 9 and 10. Random selection of hinge lines in the model experiments resulted in significant discrepancies from this relationship. For both model-generated data (based on populations A, B or C) and for the test cases, the angle between calculated and actual shear directions (approximated by the mean stretching lineation in test cases) is as large as 59°, but is more commonly less than 30°. These discrepancies may be due to the extreme sensitivity of the line of intersection to the orientation of either plane, particularly in cases of high shear strain where the angle between the two planes is very small. Alternatively, the discrepancy reflects a significant obliquity of the initial hinge line population to both the XZ plane and the shear plane (Williams 1978) (model population D, Table 2, Figs 6, 7 and 9), as might be the case if: (1) hinge lines belong to folds that pre-date shear; (2) hinge lines belong to contemporary folds that develop in a competent layer other than mylonitic foliation; or (3) hinge lines belong to contemporary folds of mylonitic foliation and the shear regime changes orientation in subsequent deformation.

CONCLUSIONS

Between Grayson County, Virginia, and Mitchell County, North Carolina, the Ashe Formation forms the hanging wall of a thrust-related ductile shear zone that is developed primarily in Grenville basement and marks the basement–Ashe boundary. Structural data from the basement–Ashe boundary zone show planar dispersion of fold-hinge lines, as is common in many ductile shear zones. The present analysis of this phenomenon leads to the following conclusions.

(1) Planar dispersion of folds may be a consequence of simple shear whereby hinge lines are variably rotated toward the shear direction.

(2) Incomplete rotation of the best-fit plane to girdle-distributed hinge lines towards mean mylonitic foliation leaves a small to moderate angle between these planes and a record of the sense of shear.

(3) An angle of 4–9° is commonly observed between the best-fit plane to hinge lines and mean mylonitic foliation, and is consistent with a theoretical model of contemporary fold rotation and the interpretation of mylonitic foliation as the shear plane.

Acknowledgements—I wish to thank J. R. Butler, K. G. Stewart, A. F. Glazner, J. M. Bartley and M. G. Steltenpohl for helpful comments and discussions during the course of this research. F. W. Vollmer, P. J. Hudleston, D. W. Rankin and an anonymous reviewer provided helpful criticism of the manuscript. This research was supported by NSF grant EAR-8518463 (awarded to J. R. Butler and S. A. Goldberg), the North Carolina Geological Survey, an On-Campus Fellowship administered by the Graduate School at UNC-CH, and grants from the Martin Trust Fund and McCarthy Memorial Trust Fund, both administered by the Department of Geology at UNC-CH.

REFERENCES

Abbott, R. N. & Raymond, L. A. 1984. The origin of the Ashe metamorphic suite, northwestern North Carolina: metamorphism and observations on geologic history. *Am J. Sci.* **284**, 350–375.

Anderson, G. M. 1976. Error propagation by the Monte Carlo method in geochemical calculations. *Geochim. cosmochim. Acta* **40**, 1533–1538.

Bak, J., Korstgard, J. & Sorensen, K. 1975. A major shear zone within the Nagssugtoqidian of west Greenland. *Tectonophysics* **27**, 191–209.

Bartholomew, M. J. & Lewis, S. E. 1984. Evolution of Grenville massifs in the Blue Ridge geologic province, central and southern Appalachians. In: *The Grenville Event in the Appalachians and Related Topics* (edited by Bartholomew, M. J.). *Spec. Pap. geol. Soc. Am.* **194**, 229–254.

Bell, T. H. 1978. Progressive deformation and reorientation of fold axes in a ductile mylonite zone; the Woodroffe thrust. *Tectonophysics* **44**, 285–320.

Bell, T. H. & Hammond, R. L. 1984. On the internal geometry of mylonite zones. *J. Geol.* **92**, 667–686.

Berthé, D., Choukroune, P. & Jegouzo, P. 1979. Orthogneiss, mylonite and noncoaxial deformation of granites: the example of the South Armorican shear zone. *J. Struct. Geol.* **1**, 31–42.

Borradaile, G. J. 1972. Variably oriented co-planar primary folds. *Geol. Mag.* **109**, 89–98.

Boyle, A. P. 1987. A model for stratigraphic and metamorphic inversions at Sulitjelma, central Scandes. *Geol. Mag.* **124**, 451–466.

Bryant, B. & Reed, J. C. Jr. 1969. Significance of lineation and minor folds near major thrust faults in the southern Appalachians and the British and Norwegian Caledonides. *Geol. Mag.* **106**, 412–429.

Bryant, B. H. & Reed, J. C. 1970. Geology of the Grandfather Mountain window and vicinity, North Carolina and Tennessee. *Prof. Pap. U.S. geol. Surv.* **615**.

Butler, J. R. 1972. Age of Paleozoic regional metamorphism in the Carolinas, Georgia and Tennessee southern Appalachians. *Am J. Sci.* **272**, 319—333.

Butler, J. R. 1973. Paleozoic deformation and metamorphism in part of the Blue Ridge thrust sheet, North Carolina. *Am J. Sci.* **273-A**, 319–333.

Butler, J. R., Goldberg, S. A. & Mies, J. W. 1987. Tectonics of the Blue Ridge west of the Grandfather Mountain window, North Carolina and Tennessee. *Geol. Soc. Am. Abs. w. Prog.* **19**, 77.

Butler, R. W. H. 1982. A structural analysis of the Moine thrust zone between Loch Eriboll and Foinaven, NW Scotland. *J. Struct. Geol.* **4**, 19–29.

Carreras, J., Estrada, A. & White, S. 1977. The effects of folding on the *c*-axis fabrics of a quartz mylonite. *Tectonophysics* **39**, 3–24.

Cheeney, R. F. 1983. *Statistical Methods in Geology*. George Allen & Unwin, London.

Christie, J. M. 1963. The Moine thrust zone in the Assynt region, northwest Scotland. *Univ. Calif. Publs geol. Sci.* **40**, 345–440.

Cobbold, P. R. & Quinquis, H. 1980. Development of sheath folds in shear regimes. *J. Struct. Geol.* **2**, 119–126.

Cook, F. A., Albaugh, D. S., Brown, L. D., Kaufman, S., Oliver, J. E. & Hatcher, R. D. Jr. 1979. Thin skinned tectonics in the crystalline southern Appalachians; COCORP seismic reflection profiling of the Blue Ridge and Piedmont. *Geology* **7**, 563–567.

Eckelman, F. D. & Kulp, J. L. 1956. The sedimentary origin and stratigraphic equivalence of the so-called Cranberry and Henderson granite in western North Carolina. *Am J. Sci.* **254**, 288–315.

Escher, A. & Watterson, J. 1974. Stretching fabrics, folds and crustal shortening. *Tectonophysics* **22**, 223–231.

Evans, D. J. & White, S. H. 1984. Microstructural and fabric studies from the rocks of the Moine Nappe, Eriboll, NW Scotland. *J. Struct. Geol.* **6**, 369–389.

Faure, M. 1985. Microtectonic evidence for eastward shear in the Jurassic orogen of SW Japan. *J. Struct. Geol.* **7**, 175–186.

Flinn, D. 1965. On the symmetry principle and the deformation ellipsoid. *Geol. Mag.* **102**, 36–45.

Fossen, H. & Rykkelid, E. 1990. Shear zone structures in the Øygarden area, west Norway. *Tectonophysics* **174**, 385–397.

Ghosh, S. K. & Sengupta, S. 1984. Successive development of plane noncylindrical folds in progressive deformation. *J. Struct. Geol.* **6**, 703–709.

Ghosh, S. K. & Sengupta, S. 1987. Progressive development of structures in a ductile shear zone. *J. Struct. Geol.* **9**, 277–287.

Glover, L., Speer, J. A., Russell, G. S. & Farrar, S. S. 1983. Ages of regional metamorphism and ductile deformation in the central and southern Appalachians. *Lithos* **16**, 223–245.

Goldstein, A. G. 1988. Factors affecting the kinematic interpretation of asymmetric boudinage in shear zones. *J. Struct. Geol.* **10**, 707–715.

Grocott, J. & Watterson, J. 1980. Strain profile of a boundary within a large ductile shear zone. *J. Struct. Geol.* **2**, 111–117.

Gulley, G. L. Jr. 1985. A Proterozoic granulite facies terrane on Roan Mountain, western Blue Ridge belt, North Carolina–Tennessee. *Bull. geol. Soc. Am.* **96**, 1428–1439.

Hansen, E. 1971. *Strain Facies*. Springer, Berlin.

Harris, L. D. & Bayer, K. C. 1979. Sequential development of the Appalachian Orogen above a master décollement—A hypothesis. *Geology* **7**, 568–572.

Hatcher, R. D., Jr. 1978. Tectonics of the western Piedmont and Blue Ridge, southern Appalachians: review and speculation. *Am J. Sci.* **278**, 276–304.

Jegouzo, P. 1980. The South Armorican shear zone. *J. Struct. Geol.* **2**, 39–47.

King, P. B. & Ferguson, H. W. 1960. Geology of northeasternmost Tennessee. *Prof. Pap. U.S. geol. Surv.* **349-C**.

La Tour, T. E. 1981. Significance of folds and mylonites at the Grenville Front in Ontario. *Bull. geol. Soc. Am.* **92**, 411–413.

Law, R. D., Casey, M. & Knipe, R. J. 1986. Kinematic and tectonic significance of microstructures and crystallographic fabrics within quartz mylonites from the Assynt and Eriboll regions of the Moine thrust zone, NW Scotland. *Trans. R. Soc. Edinb., Earth Sci.* **77**, 99–126.

Lindström, M. 1961. Beziehungen zwischen kleinen Faltenvergenzen und andern Gefügemerkmalen in den Kaledonian Skandenaviens. *Geol. Rdsch.* **51**, 144–180.

Lister, G. S. & Snoke, A. W. 1984. S–C mylonites. *J. Struct. Geol.* **6**, 617–638.

Mardia, K. V. 1972. *Statistics of Directional Data*. Academic Press, London.

Michard, A., Bouchez, J. L. & Ouazzani-Touhami, M. 1984. Obduction-related planar and linear fabrics in Oman. *J. Struct. Geol.* **6**, 36–49.

North Carolina Geological Survey. 1985. Geologic Map of North Carolina. North Carolina Division of Land Resources, Department of Natural Resources and Community Development

Passchier, C. W. & Simpson, C. 1986. Porphyroclast systems as kinematic indicators. *J. Struct. Geol.* **8**, 831–843.

Platt, J. P. 1983. Progressive refolding in ductile shear zones. *J. Struct. Geol.* **5**, 619–622.

Ramberg, H. & Ghosh, S. K. 1977. Rotation and strain of linear and planar structures in three dimensional progressive deformation. *Geology* **40**, 309–337.

Ramsay, D. M. 1979. Analysis of rotation of folds during progressive deformation. *Bull. geol. Soc. Am.* **90**, 732–738.

Ramsay, J. G. & Graham, R. H. 1970. Strain variations in shear belts. *Can. J. Earth Sci.* **7**, 786–813.

Ramsay, J. G. & Huber, M. I. 1983. *The Techniques of Modern Structural Geology, Volume* 1: *Strain Analysis*. Academic Press, London.

Rankin, D. W. 1969. The Fries fault: a major thrust in the Blue Ridge of southwestern Virginia. *Geol. Soc. Am. Abs. w. Prog.* **4**, 66.

Rankin, D. W. 1970. Stratigraphy and structure of Precambrian rocks in northwestern North Carolina. In: *Studies of Appalachian Geology. Central and Southern* (edited by Fisher, G. W. *et al.*). Interscience, New York, 227–245.

Rankin, D. W. 1971. Guide to the geology of the Blue Ridge in southwestern Virginia and northwestern North Carolina, in Guidebook to Appalachian tectonics and sulfide mineralization in southwestern Virginia. *Virginia Polytech. Inst. & State Univ. Dept geol. Sci. Guidebook* No. 5, 39–86.

Rankin, D. W. 1975. The continental margin in eastern North America in the southern Appalachians. The opening and closing of the Proto-Atlantic ocean. *Am J. Sci.* **275-A**, 296–336.

Rankin, D. W., Espenshade, G. H. & Neuman, R. B. 1972. Geologic map of the west half of the Winston–Salem quadrangle, N.C., Va., Tenn. *U.S. Geol. Surv. Misc. Geol. Invest. Map* I-709A.

Rankin, D. W., Espenshade, G. H. & Shaw, K. W. 1973. Stratigraphy and structure of the metamorphic belt in northwestern North Carolina and southwestern Virginia: a study from the Brevard fault zone to the Sauratown Mountains anticlinorium. *Am J. Sci.* **273-A**, 1–40.

Raymond, L. A., Yurkovich, S. P. & McKinney, M. 1989. Block in matrix structures in the North Carolina Blue Ridge belt and their significance for the tectonic history of the southern Appalachian orogen. In: *Melanges and Olistostromes of the U.S. Appalachians* (edited by Horton, J. W.., Jr. & Rast, N.). *Spec. Pap. geol. Soc. Am.* **228**, 195–215

Rhodes, S. & Gayer, R. A. 1977. Non-cylindrical folds, linear structures in the *X* direction and mylonite developed during translation of the Caledonian Kalak Nappe Complex of Finnmark. *Geol. Mag.* **114**, 329–341.

Sanderson, D. J. 1973. The development of fold axes oblique to the regional trend. *Tectonophysics* **16**, 55–70.

Sibson, R. H. 1977. Fault rocks and fault mechanisms. *J. geol. Soc. Lond.* **133**, 191–213.

Simpson, C. 1986. Determination of movement sense in mylonites. *J. geol. Educ.* **34**, 246–261.

Skjernaa, L. 1980. Rotation and deformation of randomly oriented planar and linear structures in progressive simple shear. *J. Struct. Geol.* **2**, 101–109.

Stose, A. J. and Stose, G. W. 1957. Geology and mineral resources of the Gossan Lead district and adjacent areas in Virginia. *Bull. Virginia Div. Miner. Resour.* **72**.

Vauchez, A., Maillet, D. & Sougy, J. 1987. Strain and deformation mechanisms in the Variscan nappes of Vendee, South Brittany, France. *J. Struct. Geol.* **9**, 31–40.

Wilcox, K. E. & Poldervaart, A. 1958. Metadolerite dike swarm in the Bakersville–Roan Mountain area, North Carolina. *Bull. geol. Soc. Am.* **69**, 1323–1367.

Williams, G. D. 1978. Rotation of contemporary folds into the *X* direction during overthrust processes in Laksfjord, Finnmark. *Tectonophysics* **48**, 29–40.